Published in final edited form as:
Hum Mutat. 2011 November ; 32(11): 1259–1267. doi:10.1002/humu.21560.

Functional Consequences and Structural Interpretation of Mutations of Human Choline Acetyltransferase

Xin-Ming Shen[1], **Thomas O. Crawford**[2], **Joan Brengman**[1], **Gyula Acsadi**[3], **Susan Iannaconne**[4], **Emin Karaca**[5], **Chaouky Khoury**[6], **Jean K. Mah**[7], **Shimon Edvardson**[8], **Zeljko Bajzer**[9], **David Rodgers**[10], and **Andrew G. Engel**[1]

[1]Department of Neurology and Muscle Research Laboratory, Mayo Clinic, Rochester, MN 55905, USA

[2]Department of Neurology and Pediatrics, John Hopkins Hospital, Baltimore, MD 21287, USA

[3]Children's Hospital of Michigan, Detroit, MI 48201, USA

[4]Department of Neurology, University of Texas Southwestern Medical Center, Dallas, TX 7529, USA

[5]Department of Medical Genetics, Ege University, Izmir, Turkey

[6]Department of Neurology, University of Oklahoma Health Sciences Center, Oklahoma City, OK 73102, USA

[7]Division of Neurology, Department of Pediatrics, University of Calgary, Calgary, Alberta, T3B 6A58C7, Canada

[8]Department of Pediatric Neurology, Hadassah University Hospital, Jerusalem, Israel

[9]Department of Biochemistry and Molecular Biology, Mayo Clinic, Rochester, MN 55905, USA

[10]Department of Molecular and Cellular Biochemistry and Center for Structural Biology, University of Kentucky, Lexington, KY 40536, USA

Abstract

Choline acetyltransferase (ChAT; EC 2.3.1.6) catalyzes synthesis of acetylcholine from acetyl-CoA and choline in cholinergic neurons. Mutations in *CHAT* (MIM # 118490) cause potentially lethal congenital myasthenic syndromes associated with episodic apnea (ChAT-CMS) (MIM # 254210). Here we analyze the functional consequences of 12 missense and 1 nonsense mutations of *CHAT* in 11 patients. Nine of the mutations are novel. We examine expression of the recombinant missense mutants in Bosc 23 cells, determine their kinetic properties and thermal stability, and interpret the functional effects of 11 mutations in the context of the atomic structural model of human ChAT. Five mutations (p.Trp421Ser, p.Ser498Pro, p.Thr553Asn, p.Ala557Thr, p.Ser572Trp) reduce enzyme expression to <50% of wild-type. Mutations with severe kinetic effects are located in the active-site tunnel (p.Met202Arg, p.Thr553Asn and p.Ala557Thr) or adjacent to the substrate binding site (p.Ser572Trp), or exert their effect allosterically (p.Trp421Ser and p.Ile689Ser). Two mutations with milder kinetic effects (p.Val136Met, p.Ala235Thr) are also predicted to act allosterically. One mutation (p.Thr608Asn) below the nucleotide binding site of CoA enhances dissociation of AcCoA from the enzyme-substrate complex. Two mutations introducing a proline residue into an α-helix (p.Ser498Pro and p.Ser704Pro) impair the thermal stability of ChAT.

Correspondence to Dr. Engel, Department of Neurology, Mayo Clinic, Rochester, MN 55905.

Keywords

Choline acetyltransferase; congenital myasthenic syndrome; enzyme kinetics; atomic structural model; thermal stability

Introduction

Congenital myasthenic syndromes (CMS) are heterogeneous disorders in which the safety margin of neuromuscular transmission is compromised by one or more specific mechanisms. The disease proteins are presynaptic, synaptic, or postsynaptic. To date, the CMS have been traced to 10 genes coding for postsynaptic proteins (*CHRNA1*, *CHRNB*, *CHRND*, *CHRNE* (reviewed by [Engel and Sine, 2005], *RAPSN* [Ohno et al., 2002], *DOK7*[Beeson et al., 2006], *MUSK* [Chevessier et al., 2004], *SCN4A* [Tsujino et al., 2003], *GFPT1* [Senderek et al., 2011], *PLEC1* [Selcen et al., 2011]) and to 3 genes coding for proteins located in the synaptic basal lamina (*COLQ* [Ohno et al., 1998], *LAMB2* [Maselli et al., 2009], *AGRIN* [Huze et al., 2009]) proteins, but only one CMS has been traced to a presynaptic protein, choline acetyltransferase encoded by *CHAT* (MIM # 118490) [Ohno et al., 2001].

ChAT (EC 2.3.1.6) catalyzes the synthesis of acetylcholine (ACh) by transfer of an acetyl group from acetyl-CoA (AcCoA) to choline in cholinergic neurons. The enzyme consists of a binding domain and a catalytic domain with an interfacial 16-Å-long active-site tunnel and a key histidine for catalytic activity at the center of the tunnel [Cai et al., 2004; Kim et al., 2006] (Fig. 1). Each domain consists of a six-stranded β-sheet surrounded by α-helices [Kim et al., 2006]. The affinity for AcCoA is much higher than for choline, and the two-substrate reaction follows sequential kinetics with AcCoA as the leading substrate of the forward reaction [Carbini and Hersh, 1993]. Although cholinergic neurons are widely distributed in the central and peripheral nervous system, all mutations in *CHAT* identified to date manifest as CMS. Because the clinical hallmark of the disease is sudden apnea, it was initially referred to as CMS with episodic apnea. *In vitro* electrophysiology studies of neuromuscular transmission in these patients revealed a progressive decrease of ACh release during subtetanic stimulation followed by prolonged recovery [Engel and Lambert, 1987; Mora et al., 1987] and pointed to *CHAT* as the candidate gene [Ohno et al., 2001]. During the past decade other disease-associated mutations of *CHAT* were reported [Maselli et al., 2003; Schmidt et al., 2003; Barisic et al., 2005; Yeung et al., 2009; Mallory et al., 2009; Schara et al., 2010] but only the first study by Ohno and coworkers examined the biochemical effects of the mutant enzymes. We here identify 1 nonsense and 12 missense mutation of *CHAT* in 11 patients. Nine mutations are novel We determine expression of the recombinant mutants, analyze their kinetic properties and thermal stability, and interpret their functional effects in the context of the atomic structural model of human ChAT at 2.2 Å resolution [Kim et al., 2005; Kim et al., 2006].

Patients, Material and Methods

Patients

All human studies described here were in accord with the guidelines of the Institutional Review Board of the Mayo Clinic. Eleven patients diagnosed with ChAT deficiency were enrolled in this study. Supp. Table S1 details the clinical features and lists the identified mutations in the 11 patients. Clinical features of Patient 7 and the mutations detected in this laboratory were previously published by Yeung et al [, 2009]. Patients 1, 2, 4, 6, and 7 presented with apnea and variable other myasthenic symptoms at birth and five (5, 8, 9, 10, 11) had their first apneic attack or experienced severe respiratory distress during the first 5 months of life. The three most severely affected patients (2, 6, and 7) were permanently

ventilator dependent. Life support was withdrawn from Patient 6 at age 10 weeks but Patients 2 and 7 are still alive at 13 and 3 years of age. Patient 4 was born with multiple joint contractures. Three siblings of Patient 6 and one sibling of Patient 3 died suddenly, and one sibling of Patient 3 was stillborn. Ten patients were treated with the cholinergic agonist pyridostigmine; six responded favorably (1, 3, 4, 5, 6, 10) but the three permanently ventilator dependent patients and patient 11 did not.

Mutation Analysis

DNA was isolated from blood by standard methods. We directly sequenced all exons and flanking noncoding regions as well as the unique S, R, N, and M exons of *CHAT*. Nucleotide numbering reflects cDNA numbering with +1 corresponding to the A of the translation initiation codon ATG of M type *CHAT* (RefSeq. NM_020549.4) encoding 83 kDa ChAT. Codon numbers start from the translation initiation codon according to the reference sequence NP_065574. We used the 83-kDa human ChAT protein encoded by the M transcript for numbering amino acids because it covers all coding regions of *CHAT* and allows designation of any mutation in the three open reading frames of the transcript. [Ohno et al., 2001] We searched for the identified mutations in family members by DNA sequencing and in normal controls by allele specific PCR. In Patient 5 and his family members relative quantitation of *CHAT* exons S, 11 and 17 was performed by a quantitative RT-PCR. The primer sequences are available upon request.

Construction of Expression Vectors

We used the S transcripts of *CHAT* for expression studies because its open reading frame is encoded by all *CHAT* transcripts, it harbors all identified mutations, and was previously cloned by us from a spinal cord cDNA library[Ohno et al., 2001] predicting it is the transcript used by motor neurons. Construction of the mammalian cell expression vector pRBG4 containing the 74-kDa S-transcript (NM_ 001142933; nucleotides 470-2470) and the bacterial-expression vector pRT7/NT containing the 70-kDa S-transcript (NM_001142934.1; nucleotides 578-2470) of wild-type ChAT were previously described [Ohno et al., 2001]. The identified mutations in *CHAT* were introduced into both vectors using the QuikChange Site-Directed Mutagenesis kit (Agilent). Presence of desired mutations and absence of unwanted mutations was confirmed by sequencing the entire inserts.

Protein Expression in Bosc 23 Cells

Bosc 23 cells were transfected with 1 μg of the long S isoform of wild-type and mutant *CHAT* cDNA and 1 μg of the pSV-β-galactosidase control vector (Promega) per 35 mm dish using *Trans*IT-LT1 (Mires Bio) following the manufacturer's instruction. Bosc 23 cells were extracted 2–3 days after transfection and the cell lysates were immunoblotted as previously described [Ohno et al., 2001]. Plate to plate variations of transfection efficiency were corrected by monitoring the expression of β-galactosidase in the immunoblots.

Expression and Purification of Recombinant CHAT Expressed in Bacteria

BL21(DE3)pLysS bacteria (Invitrogen) were transformed with wild-type and mutant *CHAT* cDNA in pCRT7/NT and grown at 37°C in 2 ml LB medium containing 100 μg/ml ampicillin and 34 μg/ml chloramphenicol. After an overnight growth, the bacterial lysates were purified on a Ni-agarose column and then further purified by fast protein liquid chromatography. Details of the procedure are shown in Supplemental File 1.

Measurement of Enzyme Activity and Treatment of Kinetic Data

ChAT velocity was measured under steady state conditions over a range of choline and AcCoA concentrations in a 36-point assay using the radiochemical method of Fonnum [1975]. We first analyzed the two-substrate ChAT reaction by assuming an ordered random bi-bi mechanism described by the steady state equation [Segel, 1975].

$$v=k_{cat}[E][A][B]/(K_{iA}K_{mB}+K_{mB}[A]+K_{mA}[B]+[A][B]) \quad \text{Equation 1}$$

where v is the initial reaction velocity, A corresponds to AcCoA, B to choline, and E to ChAT, k_{cat} represents the turnover number ($V_{max}/[E]$), K_{iA} the dissociation constant for the E-A complex, and K_{mA} and K_{mB} the Michaelis-Menten constants. The initial steps of the reaction are schematically represented by the scheme below [Segel, 1975],

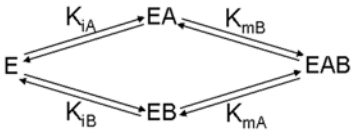

and according to the law of equilibrium

$$K_{iA}K_{mB}=K_{iB}K_{mA} \quad \text{Equation 2}$$

where K_{iB} is the dissociation constant for the E-B complex.

Examination of Lineweaver-Burke plots of 1/v as a function of 1/[AcCoA] revealed that for 8 mutations (p.Val136Met, p.Met202Arg, p.Ala235Thr, p.Trp421Ser, p.Ser498Pro, pAla631Thr, p.Ile689Ser, and p.Ser704P) high concentrations of AcCoA inhibited the reaction at low choline concentrations. To correct for this, Equation 1 was modified to allow for the formation of a ChAT-$(AcCoA)_2$ dead-end complex [Segel, 1975]

$$v=K_{cat}[E][A][B]/(K_{iA}K_{mB}+K_{mB}[A](1+[A]/K_{isA})+K_{mA}[B]+[A][B]) \quad \text{Equation 3}$$

where K_{iA} is the dissociation constant for the E-A complex and K_{isA} the dissociation constant for the dead-end complex. Comparison of the results obtained by Equation 1 and 2 by the F-test on chi-square indicated that the additional term added to the Equation 1 significantly improved the fits [Cook and Weisberg, 1990; Buckwitz and HolzHütter, 1990] except for three mutants (p.Thr553Asn, p.Ala557, and p.Ser572Trp) discussed below.

The kinetic activities of the p.Thr608Asn mutant were analyzed using Equation 1.

For the p.Thr553Asn and p.Ala557Thr mutants, the choline concentration obtainable in the reaction system was much lower than K_{mB}. Therefore Equation 1 reduces to

$$v=(k_{cat}/K_{mB})[E][A][B]/(K_{iA}+[A]) \quad \text{Equation 4}$$

Similarly, for the p.Ser572Trp mutant the obtainable concentration of AcCoA is much lower than K_{mA}, and Equation 1 reduces to

$$v=(k_{cat}/K_{mA})[E][A][B]/(K_{iB}+[B]) \quad \text{Equation 5}$$

Here K_{iB} is substituted for $K_{iA}K_{mB}/K_{mA}$ according to Equation 2..

Sigmaplot 10 computer program (SPSS, Chicago) and weighted nonlinear regression were used to generate the kinetic constants for each enzyme by fitting the data to the above equations.

Thermal Denaturation Studies

Prior to measuring thermal denaturation values, ChAT samples were diluted to 0.5 mg/ml in 10 mM Tris (pH 7.4), 2 mM NaCl, 0.1 mM DTT. Thermal denaturation was monitored by increasing the temperature at a rate of 1 °C/min and measuring the circular dichroism signal at 222 nm with a Jasco J-810 spectropolarimeter (Easton, MD) as a function of sample temperature in the range of 10–70 °C. T_m values were determined by fitting thermal denaturation curves to a Boltzmann sigmoid function.

Results

Mutation Analysis

We identified 12 missense and one nonsense mutations in *CHAT* in 11 kinships (Table 1, Fig. 1, and Supp. Figure S1). Nine mutations are novel; p.Thr553Asn and p.Ser704Pro detected in this laboratory were published but not functionally characterized by Yeung et al [, 2009]. p.Ala557Thr was previously reported by Mallory et al [2009]. None of the mutations was detected in 200 to 400 alleles of unrelated control subjects. All mutated residues are conserved in dog, mouse, rat, and chicken. Four residues (Met202, Trp421, Thr553, and Ala557) are also conserved in *Drosophila* and *C. elegans*.

p.Val136Met was observed in three patients (2, 6, and 9) and p.Ala557Thr in five (3, 5, 8, 9, and 10). Patient 8 is homozygous for p.Ala557Thr. Patient 5 showed apparent homozygosity for p.Ala557Thr but the mutation was transmitted by the unaffected mother and not carried by the father (see Supp. Figure S1). Quantitative RT-PCR revealed the patient, her father and one brother are hemizygous for *CHAT*. One unaffected sibling inherited the wild-type allele from both parents; the other unaffected sibling inherited only the maternal wild-type allele (see Supp. Figure S2). p.Ala557Thr also determines the phenotype in patient 10 who carries a nonsense mutation on her second allele. Patient 11, born to consanguineous parents, is homozygous for p.Ile689Ser.

Expression, Kinetic Properties, and Thermal Stability of Wild-Type and Mutant ChATs

To examine the expression of the missense mutants at the protein level, we genetically engineered mutant and wild-type *CHAT* cDNAs into Bosc 23 cells and analyzed immunoblots of cell lysates. The spinal cord (S-type) ChAT transcript has two alternative start sites that yield 70 kDa and 74 kDa proteins at a constant ratio [Ohno et al., 2001]. Eight mutants expressed at significantly lower levels than wild-type, and five of these (p.Trp421Ser, p.Ser498Pro, p.Thr553Asn, p.Ala557Thr, p.Ser572Trp) expressed at <50% of wild-type (Fig. 2 and Tables 1 and 2).

To evaluate the kinetic parameters and thermal stability of wild-type and mutant ChATs, we transformed *E. coli* with histidine-tagged *CHAT* cDNAs and purified the enzymes recovered from the bacterial cell lysates on a Ni-NTA column followed by fast protein liquid chromatography. Ten mutations alter one or more rate constants of ChAT activation and two mutations compromise the thermal stability of the mutant protein (Tables 1 and 2). The Discussion analyzes the effects of each mutation and interprets them in the context of the atomic structural model of ChAT.

Discussion

Mutations Lining the Active Site Tunnel

Four mutations, p.Met202Arg, p.Ala557Thr, p.Glu555X and p.Thr553Asn involve residues that line the active-site tunnel (Fig. 3). p.Glu555X is predicted to abrogate enzyme activity. p.Met202Arg reduces the k_{cat} ~40-fold and the overall catalytic efficiency ~100-fold (Table 2 and Fig. 3A). The mutated methionine is separated only by Tyr203 from the key catalytic His442. Moreover, Met202 along with Tyr203 are on a coil region that connects the binding to the catalytic domain and is subject to conformational change during catalysis [Kim et al., 2006]. Replacement of the neutral side chain of Met by the longer and basic side chain of Arg likely disrupts the local structure of the active site, including the conformation of the side chain of the catalytic His442, and hinders conformational change during catalysis.

The p.Thr553Asn and p.Ala557Thr mutants show only slight saturation with AcCoA concentrations and no saturation with choline, indicating an extremely low affinity for AcCoA and choline (Table 2 and Fig. 3A). The mutated residues are in the splayed β sheet 11 that forms part of the active-site tunnel. Their side chains point away from the active-site tunnel but mutation of either residue likely perturbs the local environment by disrupting the conformations of the nearby Tyr554 and Ser558 essential for choline and AcCoA binding [Dobransky et al., 2001; Kim et al., 2006].

Mutation Near the Substrate Binding Site

p.Ser572Trp dramatically curtails affinity and catalytic efficiency for AcCoA and choline (Table 2). Ser572 is located in the core of the enzyme below the sheet that contains Tyr554 and Ser558 which are directly involved in substrate binding (Fig. 3B). Conversion of Ser to bulky Trp disrupts the core and likely affects positions of these critical residues.

p.Thr608Asn enhances dissociation of AcCoA from the enzyme complex by 3.5-fold and reduces the overall catalytic efficiency to 39% of wild-type (Table 2). Although Thr608 does not interact with AcCoA directly, it is positioned just below the binding site for the nucleotide portion of CoA (Fig. 4A). It is also 4 Å from Gln262, which interacts with CoA phosphates in the P loop covering the CoA binding site, and is 3.7 Å from Ser530 and 3.3 Å from Thr611 which interact with CoA.

Mutations Distant from Active or Substrate Binding Sites

The mutations in this group include p.Trp421Ser and p.Ile689Ser with severe kinetic effects, and p.Val136Met, p.Ala235Thr and p.Thr608Asn with milder kinetic effects..

Although Trp421 is 19Å from the catalytic His442, the k_{cat} of the mutant enzyme is <1% of wild-type and the dissociation constant of AcCoA from the enzyme-substrate complex is enhanced 4-fold (Table 2). We postulate the structural perturbation caused by the p.Trp421Ser affects the active site allosterically because it is adjacent to Tyr422 which is only 3.3 Å from Glu441 that links to His442 (Fig. 4B). The side chain of Trp421 points into hydrophobic/aromatic core of the enzyme and accepts a hydrogen bond from the nearby γ-oxygen of Tyr280. Also, the serine replacing Trp421 cannot make the hydrogen bond nor fill the pocket left by tryptophan. This may alter folding and account for the reduced expression of the mutant enzyme.

Ile689 is 18 Å from the catalytic His442 but p.Ile689Ser reduces k_{cat} to 27% of wild-type (Table 2). Ile689 is at the beginning of β strand 16 which is antiparallel to β strand 15 (Fig. 4C). The side chain of Ile689 extends into hydrophobic core, and replacement of Ile689 by Ser likely disrupts the packing locally. We postulate the mutation exerts its effect by altering

positioning of β strand 16 that forms one side of the active site cavity. Beta strand 16 is linked by a bridge between Cys692 to Cys681 on antiparallel β strand 15, or with Cys668 on β strand 14, and both residues are in the cluster of cysteine residues involved in the formation of the active complex [Kim et al., 2006]. Thus a small change in positioning of β strand 16 likely affects alignment of the bound substrates relative to the catalytic histidine residue and thereby the catalytic rate.

The p.Val136Met mutant has a T_m is 2°C lower than wild-type, indicating a mild decrease in thermal stability. Val136 is close to the N-terminal end of ChAT and remote from substrate binding or catalytic sites. However, the mutation enhances dissociation of AcCoA from the enzyme complex and thereby reduces the overall catalytic efficiency of ChAT to ~25% of wild-type (Table 2). A plausible explanation for this would be an energetic link between Val136 and residues contributing to the AcCoA binding site via Val136-Trp193-Asn622-Val567-Ser558 with interresidue distances ranging from 3.4 to 4.4 Å (Fig. 5A).

p.Ala235Thr is in α helix 7 and 25 Å from the catalytic His442 (Fig. 5B). The mutation has only a slight effect on thermal stability but decreases the k_{cat} to 43%, and the overall catalytic efficiency to ~45%, of wild-type (Table 2). Ala235 is 4.2 Å from Val430 on β strand 7 which is antiparallel to β strand 8 that connects to His442. Replacement of neutral Ala235 by the larger and polar Thr likely displaces the antiparallel β strands and consequently His442.

p.Ala631Thr reduces expression, affinity for AcCoA, and overall catalytic efficiency of ChAT to 70% of wild-type. Ala631 is 27 Å from the active site and a path to the active site is not apparent. A possible explanation for the observed kinetic effects would be altered folding of the mutant enzyme but its T_m is unaltered.

Mutations Affecting the Thermal Stability of ChAT

This group includes two mutations that introduce a Pro residue into an α helix. p.Ser498Pro is 23 Å from the active site. It expresses at ~30% of wild-type and decreases k_{cat} to ~70% of wild-type (Table 2). In addition, Ser498 is in α helix 15 which is only 2.9 Å from Asp356 that links α helix 10 to 11 (Fig. 6A), predicting an effect on the stability of ChAT, and thermal denaturation studies reveal a large decrease in T_m relative to wild-type (Table 2 and Fig. 6C).

p.Ser704Pro is 18 Å from the active site. It is located at the beginning of α helix 24 and its side chain forms a hydrogen bond with Ser695 in β strand 16 (Fig. 6B). The mutation does not significantly change the expression or kinetic properties of ChAT but its position in an α helix predicts an effect on the folding or thermal stability of ChAT. We confirmed this by thermal denaturation studies that reveal a large decrease in T_m relative to wild-type (Table 2 and Fig. 6C).

Genotype-Phenotype Correlations

Genotype-phenotype correlations are hindered in patients with biallelic mutations. However, it is noteworthy that the most severely affected Patients (2, 6, and 7) with life-long apnea and severe weakness refractory to pyridostigmine harbor one mutation near the active-site of the enzyme (p.Ser572Trp, p.Met202Arg, and p.Thr553Asn) (Fig. 3A). The second mutation in Patients 2 and 6, p.Val136Met, expresses at <50% of wild-type and reduces the overall catalytic efficiency of the enzyme to 24% (Table 2). The second mutation in Patient 7, p.Ser704Pro, renders the enzyme conformationally unstable (Fig. 6B and C).

Patient 1 is heterozygous for p.Thr421Ser (Fig. 4B) and p.Ala631Thr. The p.Thr421Ser mutation reduces the k_{cat} of the enzyme to <1% of wild-type; therefore p.Ala631Thr, which

reduces the expression and overall catalytic efficiency to ~70 % of wild-type, dominates the clinical phenotype (Table 2). The patient was severely affected as an infant but responded well to pyridostigmine.

The p.Ile689Ser mutation also has severe kinetic consequences (Fig. 4C). Patient 11 is homozygous for this mutation and is severely affected; he is refractory to pyridostigmine and has frequent episodes of hypoventilation. On the other hand, Patients 5, 8, and 10 whose phenotype is determined by the p.Ala557Thr mutation, which is also near the active site, are less severely affected and remain responsive to pyridostigmine.

Clinical Implications

Among the genetically distinct CMSs identified to date, ChAT-CMS is one of the most disabling and lethal. Five of the 11 patients in our series did not respond or responded poorly to pyridostigmine, while in five similar treatment was beneficial. Therefore a trial of cholinesterase inhibitors must be part of the initial management of all CMS-ChAT patients.

The permanent paralysis and refractoriness to therapy of the three most severely affected patients indicates that the amount of ACh released from the nerve terminal during activity generates endplate potentials subthreshold for triggering propagated action potentials even when cholinesterase inhibition by pyridostigmine prolongs the lifetime of ACh in the synaptic space.

Other types of CMS can also be highly disabling. These include endplate acetylcholinesterase deficiency caused by mutations in *COLQ* [Ohno et al., 2000; Shapira et al., 2002], fast-channel mutations of AChR subunits that severely impede gating [Shen et al., 2003; Brownlow et al., 2001], and low-expressor or null mutations of both alleles of *CHRNA1*, *CHRNB*, *CHRND* coding for non-ε subunits of AChR [Engel et al., 2009] as well as defects in rapsyn encoded by *RAPSN* [Ohno et al., 2002; Burke et al., 2003; Dunne and Maselli, 2003; Muller et al., 2006] and in $Na_v1.4$ encoded by *SCN4A* [Tsujino et al., 2003]. However, if correctly diagnosed, these CMS can be at least partially improved by pharmacotherapy [Engel, 2007].

Supplementary Material

Refer to Web version on PubMed Central for supplementary material.

Acknowledgments

This work was supported by NIH Grants NS6277 and by a Research Grant by the Muscular Dystrophy Association (to A.G. Engel) and by NIH grants NS38041, DA02243, P20 RR20171 (to D. Rodgers).

Reference List

1. Barisic N, Muller JS, Paucic-Kirincic E, Gazdik M, Lah-Tomulic K, Pertl A, Sertic J, Zurak N, Lochmuller H, Abicht A. Clinical variability of CMS-EA (congenital myasthenic syndrome with episodic apnea) due to identical CHAT mutations in two infants. Eur J Paediatr Neurol. 2005; 9:7–12. [PubMed: 15701560]
2. Beeson D, Higuchi O, Palace J, Cossins J, Spearman H, Maxwell S, Newsom-Davis J, Burke G, Fawcett P, Motomura M, Muller J, Lochmuller H, Slater C, Vincent A, Yamanashi Y. Dok-7 mutations underlie a neuromuscular junction synaptopathy. Science. 2006; 313:1975–1978. [PubMed: 16917026]
3. Brownlow S, Webster R, Croxen R, Brydson M, Neville B, Lin J-P, Vincent A, Newsom-Davis J, Beeson D. Acetylcholine receptor δ subunit mutations underlie a fast-channel myasthenic syndrome and arthrogryposis multiplex congenita. J Clin Invest. 2001; 108:125–130. [PubMed: 11435464]

4. Buckwitz D, HolzHütter H-G. A new method to discriminate between enzyme-kinetic models. Computers, Math Applic. 1990; 20:117–126.
5. Burke G, Cossins J, Maxwell S, Owens G, Vincent A, Robb S, Nicolle M, Hilton-Jones D, Newsom-Davis J, Palace J, Beeson D. Rapsyn mutations in hereditary myasthenia. Distinct early- and late-onset phenotypes. Neurology. 2003; 61:826–828. [PubMed: 14504330]
6. Cai Y, Cronin CN, Engel AG, Ohno K, Hersh LB, Rodgers D. Choline acetyltransferase structure reveals distribution of mutations that cause motor disorders. EMBO J. 2004; 23:2047–2058. [PubMed: 15131697]
7. Carbini LA, Hersh LB. Functional analysis of conserved histidines in choline acetyltransferase by site-directed mutagenesis. J Neurochem. 1993; 61:247–253. [PubMed: 8515270]
8. Chevessier F, Faraut B, Ravel-Chapuis A, Richard P, Gaudon K, Bauche S, Prioleau C, Herbst R, Goillot E, Ioos C, Azulay JP, Attarian S, Leroy J-P, Fournier E, Legay C, Schaeffer L, Koenig J, Fardeau M, Eymard B, Pouget J, Hantai D. MUSK, a new target for mutations causing congenital myasthenic syndrome. Hum Mol Genet. 2004; 13:3229–3240. [PubMed: 15496425]
9. Cook, RD.; Weisberg, S. Linear and nonlinear regression. In: Berry, DA., editor. Statistical Methodology in the Pharmaceutical Sciences. New York: Marcel Decker; 1990. p. 163-199.
10. Dobransky T, Davis WL, Rylett RJ. Functional characterization of phosphorylation of 69-kDa human choline acetyltransferase at serine 440 by protein kinase C. J Biol Chem. 2001; 276:22244–22250. [PubMed: 11303024]
11. Dunne V, Maselli RA. Identification of pathogenic mutations in the human rapsyn gene. Hum Genet. 2003; 48:204–207.
12. Engel AG. The therapy of congenital myasthenic syndromes. Neurotherapeutics. 2007; 4:252–257. [PubMed: 17395135]
13. Engel AG, Lambert EH. Congenital myasthenic syndromes. Electroencephalogr Clin Neurophysiol Suppl. 1987; 39:91–102. [PubMed: 2443341]
14. Engel AG, Shen X-M, Selcen D. What have we learned from the congenital myasthenic syndromes? J Mol Neurosci. 2009; 40:143–153. [PubMed: 19688192]
15. Engel AG, Sine SM. Current understanding of congenital myasthenic syndromes. Curr Opin Pharmacol. 2005; 5:308–321. [PubMed: 15907919]
16. Fonnum F. A rapid radiochemical method for the determination of choline acetyltransferase. J Neurochem. 1975; 24:407–409. [PubMed: 1113118]
17. Huze C, Bauche S, Richard P, Chevessier F, Goillot E, Gaudon K, Ben AA, Chaboud A, Grosjean I, Lecuyer HA, Bernard V, Rouche A, Alexandri N, Kuntzer T, Fardeau M, Fournier E, Brancaccio A, Ruegg MA, Koenig J, Eymard B, Schaeffer L, Hantai D. Identification of an agrin mutation that causes congenital myasthenia and affects synapse function. Am J Hum Genet. 2009; 85:155–167. [PubMed: 19631309]
18. Kim AR, Dobransky T, Rylett RJ, Shilton BH. Surface-entropy reduction used in the crystallization of human choline acetyltransferase. Acta Crystallogr Sect D. 2005; 61:1306–1310. [PubMed: 16131766]
19. Kim A-R, Rylett RJ, Shilton BH. Substrate binding and catalytic mechanism of human acetylcholine transferase. Biochemistry. 2006; 45:14621–14631. [PubMed: 17144655]
20. Mallory SA, Shaw JG, Burgess SL, Estrella E, Nurko S, Burpee TM, et al. Congenital myasthenic syndrome with episodic apnea. Pediatr Neurol. 2009; 41:42–45. [PubMed: 19520274]
21. Maselli RA, Chen D, Mo D, Bowe C, Fenton G, Wollman RL. Choline acetyltransferase mutations in myasthenic syndrome due to deficient acetylcholine resynthesis. Muscle Nerve. 2003; 27:180–187. [PubMed: 12548525]
22. Maselli RA, Ng JJ, Andreson JA, Cagney O, Arredondo J, Williams C, Wessel HB, Abdel-Hamid J, Wollmann RL. Mutations in *LAMB2* causing a severe form of synaptic congenital myasthenic syndrome. J Med Genet. 2009; 46:203–208. [PubMed: 19251977]
23. Mora M, Lambert EH, Engel AG. Synaptic vesicle abnormality in familial infantile myasthenia. Neurology. 1987; 37:206–214. [PubMed: 3027611]
24. Muller JS, Baumeister SK, Schara U, Cossins J, Krause S, von der Hagen M, Huebner A, Webster R, Beeson D, Lochmuller H, Abicht A. Impaired receptor clustering in congenital myasthenic syndrome with novel RAPSN mutations. Brain. 2006; 129:2784–2793. [PubMed: 16916845]

25. Ohno K, Brengman JM, Tsujino A, Engel AG. Human endplate acetylcholinesterase deficiency caused by mutations in the collagen-like tail subunit (ColQ) of the asymmetric enzyme. Proc Natl Acad Sci USA. 1998; 95:9654–9659. [PubMed: 9689136]
26. Ohno K, Engel AG, Brengman JM, Harper CM, Shen X-M, Heidenreich FR, Vincent A, Milone M, Tan E, Demirci M, Walsh P, Nakano S, Akiguchi I. The spectrum of mutations causing endplate acetylcholinesterase deficiency. Ann Neurol. 2000; 47:162–170. [PubMed: 10665486]
27. Ohno K, Engel AG, Shen X-M, Selcen D, Brengman JM, Harper CM, Tsujino A, Milone M. Rapsyn mutations in humans cause endplate acetylcholine receptor deficiency and myasthenic syndrome. Am J Hum Genet. 2002; 70:875–885. [PubMed: 11791205]
28. Ohno K, Tsujino A, Shen XM, Brengman J, Harper CM, Bajzer Z, Udd B, Beyring R, Robb S, Kirham FJ, Engel AG. Choline acetyltransferase mutations cause myasthenic syndrome associated with episodic apnea in humans. Proc Natl Acad Sci USA. 2001; 98:2017–2022. [PubMed: 11172068]
29. Schara U, Christen H-J, Durmus H, Hietala M, Krabetz K, Rodolico C, et al. Long-term follow-up in patients with congenital myasthenic syndrome due to CHAT mutations. Eur J Paediatr Neurol. 2010; 14:326–333. [PubMed: 19900826]
30. Schmidt C, Abicht A, Krampfl K, Voss W, Stucka R, Mildner G, Petrova S, Schara U, Mortier W, Bufler J, Huebner A, Lochmüller H. Congenital myasthenic syndrome due to a novel missense mutation in the gene encoding choline acetyltransferase. Neuromuscul Disord. 2003; 13:245–251. [PubMed: 12609506]
31. Segel, IH. Steady-state kinetics of multireactant enzymes. In: Segel, IH., editor. Enzyme Kinetics. New York: John Wiley & Sons; 1975. p. 505-845.
32. Selcen D, Juel VC, Hobson-Webb LD, Smith EC, Stickler DE, Bite AV, Ohno K, Engel AG. Myasthenic syndrome caused by plectinopathy. Neurology. 2011; 76:327–336. [PubMed: 21263134]
33. Senderek J, Muller JS, Dusl M, Strom TM, et al. Hexosamine biosynthetic pathway mutations cause neuromuscular transmission defect. Am J Hum Genet. 2011; 88:162–172. [PubMed: 21310273]
34. Shapira YA, Sadeh ME, Bergtraum MP, Tsujino A, Ohno K, Shen X-M, Brengman JM, Edwardson S, Matoh I, Engel AG. Three novel *COLQ* mutations and variation of phenotypic expressivity due to G240X. Neurology. 2002; 58:603–609. [PubMed: 11865139]
35. Shen X-M, Ohno K, Tsujino A, Brengman JM, Gingold M, Sine SM, Engel AG. Mutation causing severe myasthenia reveals functional asymmetry of AChR signature Cys-loops in agonist binding and gating. J Clin Invest. 2003; 111:497–505. [PubMed: 12588888]
36. Tsujino A, Maertens C, Ohno K, Shen X-M, Fukuda T, Harper CM, Cannon SC, Engel AG. Myasthenic syndrome caused by mutation of the *SCN4A* sodium channel. Proc Natl Acad Sci USA. 2003; 100:7377–7382. [PubMed: 12766226]
37. Yeung WL, Lam CW, Fung LWE, Hon KLE, Ng PC. Severe congenital myasthenia gravis of the presynaptic type with choline acetyltransferase mutation in a Chinese infant with respiratory failure. Neonatalogy. 2009; 95:183–186.

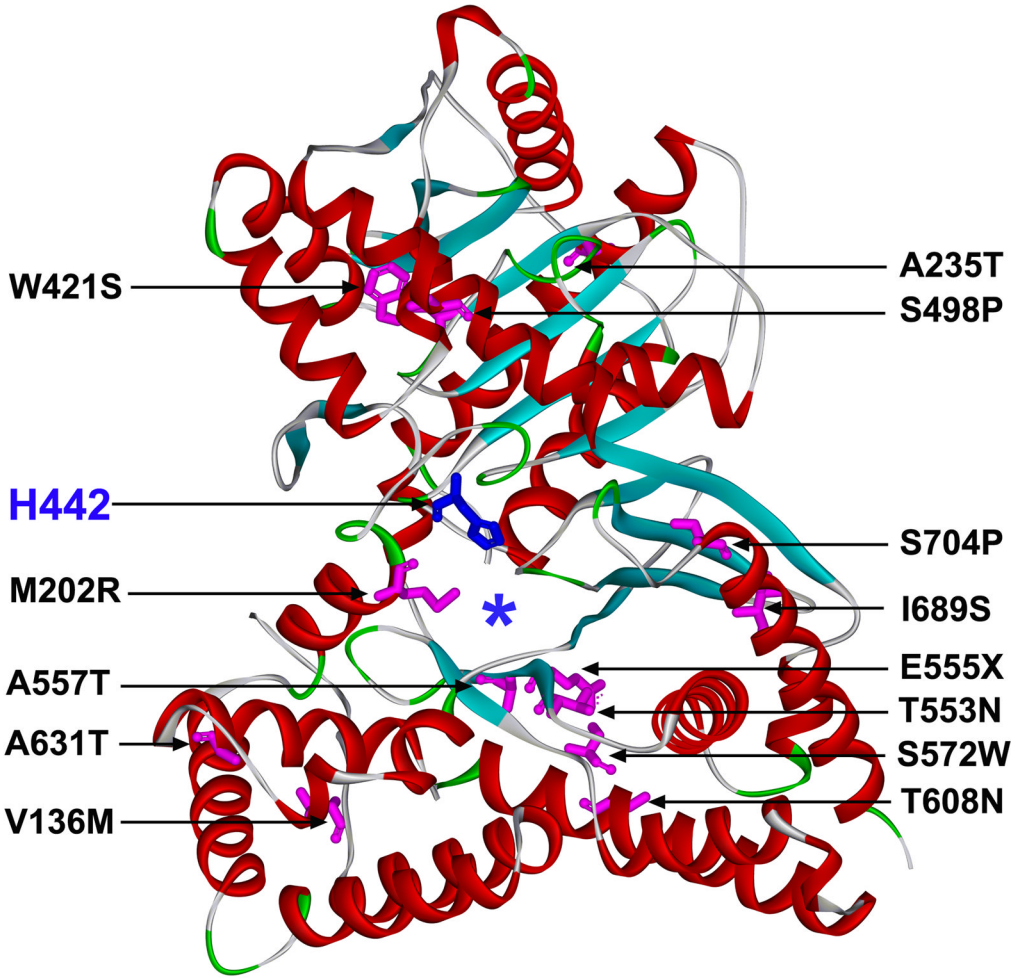

Fig. 1.
Structure of human ChAT showing the identified mutations and the catalytic His-442 at the active site. Asterisk indicates the active-site tunnel. (PDB 2FY2).

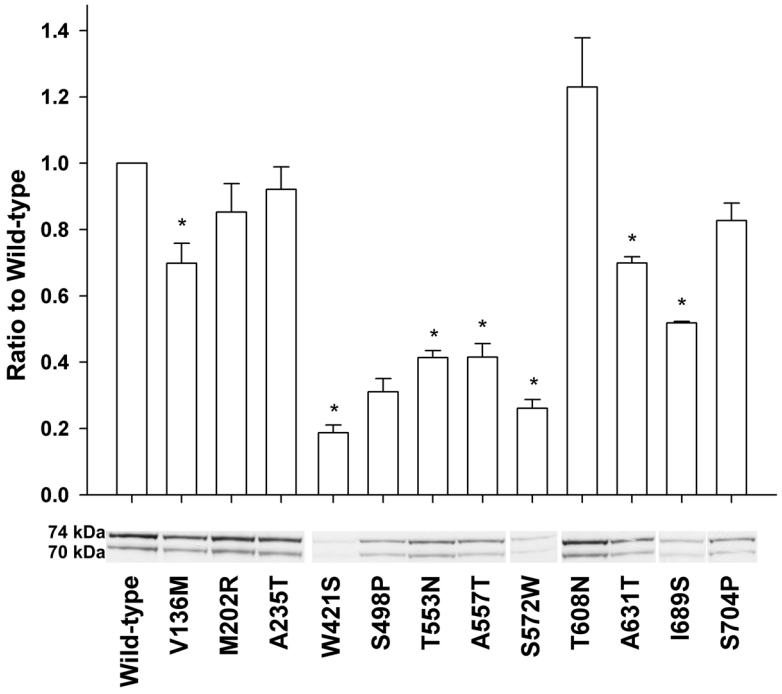

Fig. 2.

Immunoblot demonstrating expression of wild-type and mutant ChATs in Bosc 23 cells. All samples were loaded on the same gel and the identified bands rearranged to match the indicated sequence of mutations. Expression levels are normalized for expression of cotransfected β-galactosidase and by comparison to wild-type. Bars and lines indicate mean and SE of 3 to 4 transfections. Asterisks indicates difference from wild-type with $P < 0.001$ except for p.Val136Met where P is <0.05.

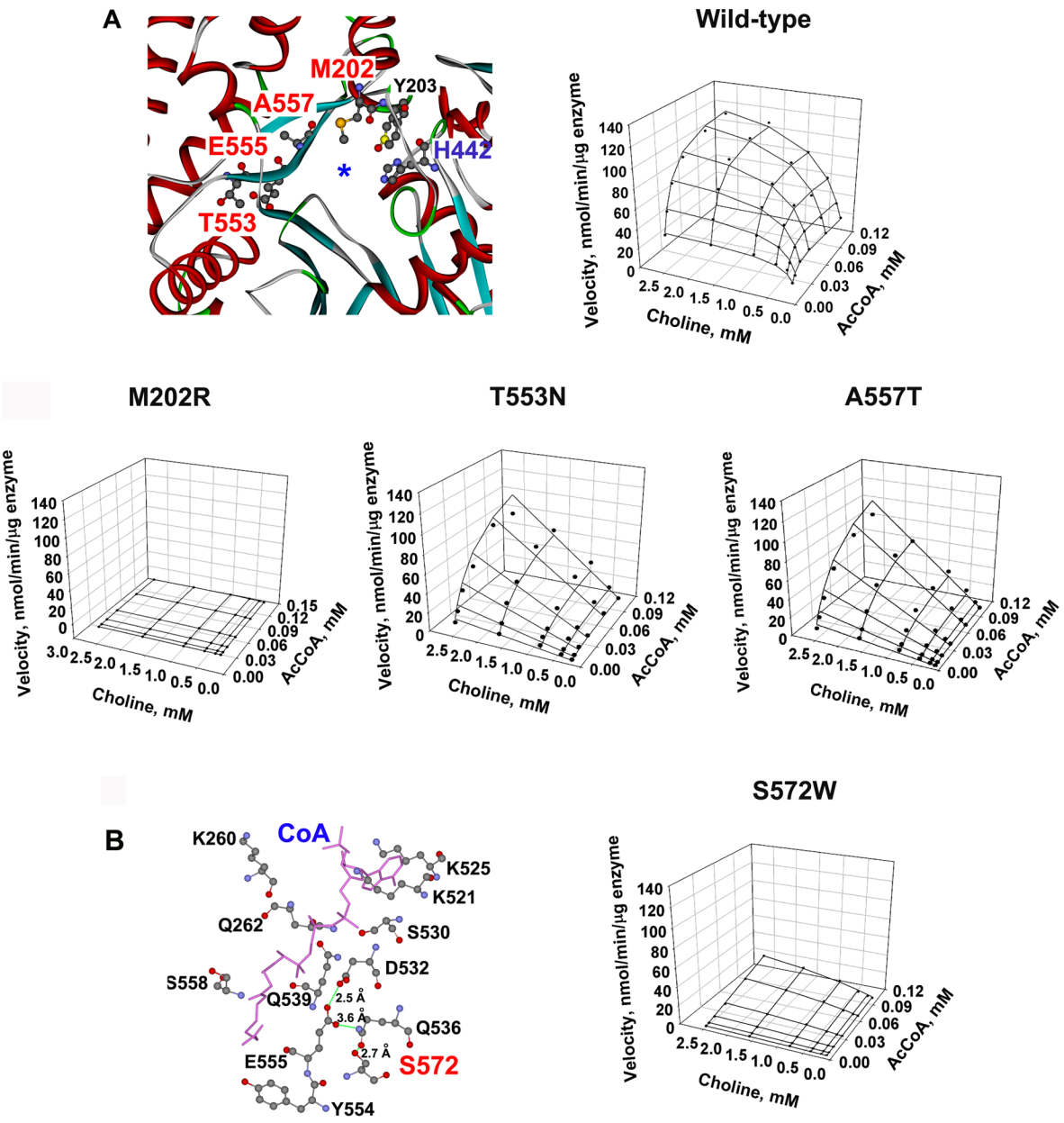

Fig. 3.

(A) Positions of mutated residues in the active site tunnel and kinetic landscapes of wild-type and mutant enzymes. The p.M202R mutant is essentially inactive. T553N and A557T mutants fail to saturate within the indicated range of substrate concentrations. (B) Position of Ser572 and kinetic landscape of the p.Ser572Trp-ChAT. Ser 572 is close to the AcCoA and choline binding sites. The mutation markedly reduces k_{cat} and K_m for both substrates.

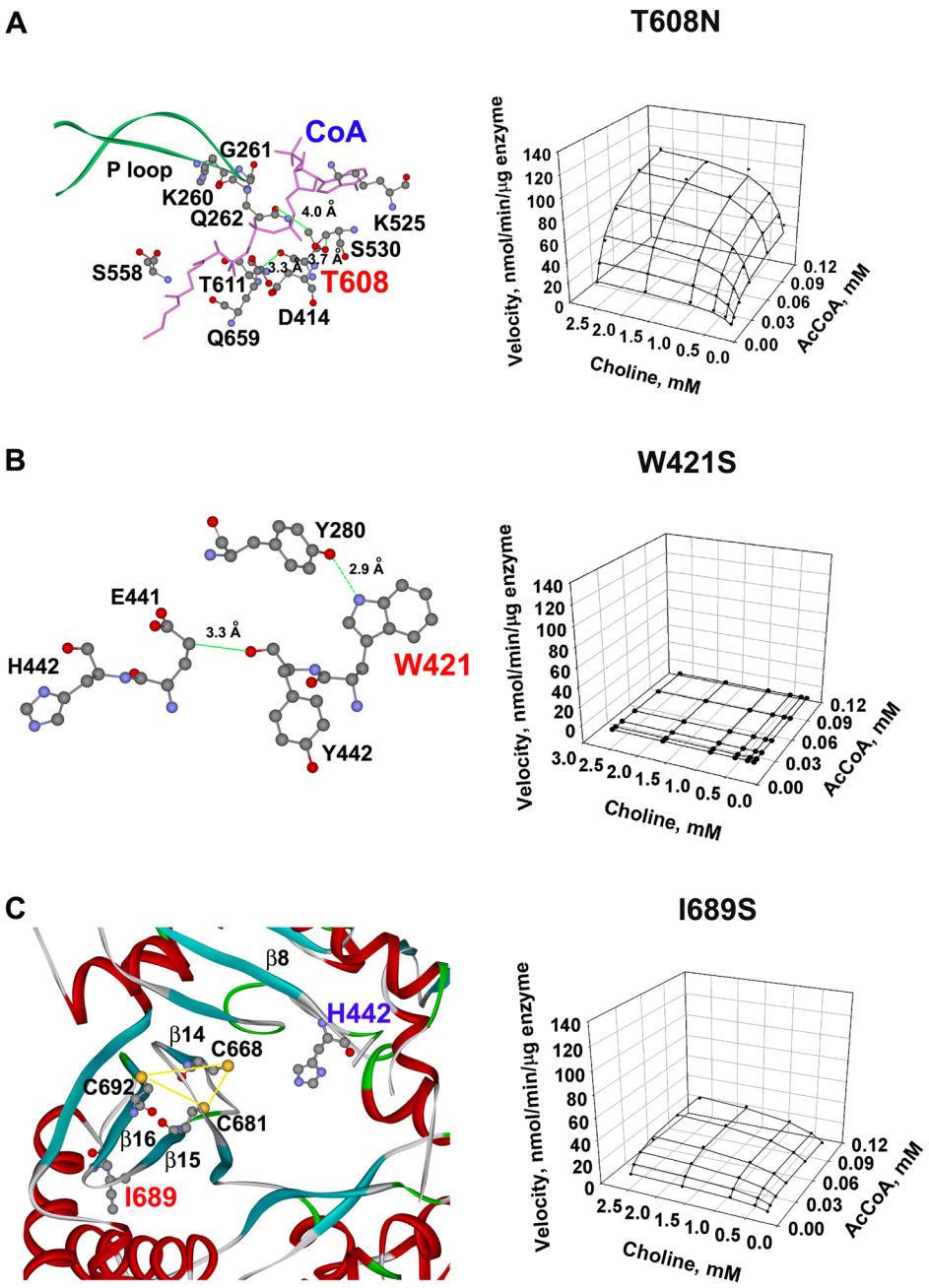

Fig. 4.

(A) Position of Thr608 near the AcCoA binding site and kinetic landscape of p.Thr608Asn-ChAT. The main effect of the mutation is to enhance the dissociation constant of AcCoA (K_{iA}) from the enzyme-substrate complex by 3.5-fold. (B) p.Trp421 and its neighboring residues, and the kinetic landscape of p.Trp421Ser-ChAT. The mutation reduces the k_{cat} to <1% of wild-type. The predicted path from Trp421 to His442 is via Tyr422 and Glu441. (C) Position of Ile689 and the kinetic landscape of pr.Ile689Ser-ChAT. The main effect of the mutation is to curtail k_{cat} to 27% of wild-type. The mutation is predicted to alter the position of β-strand 16 that forms one side of the active site cavity.

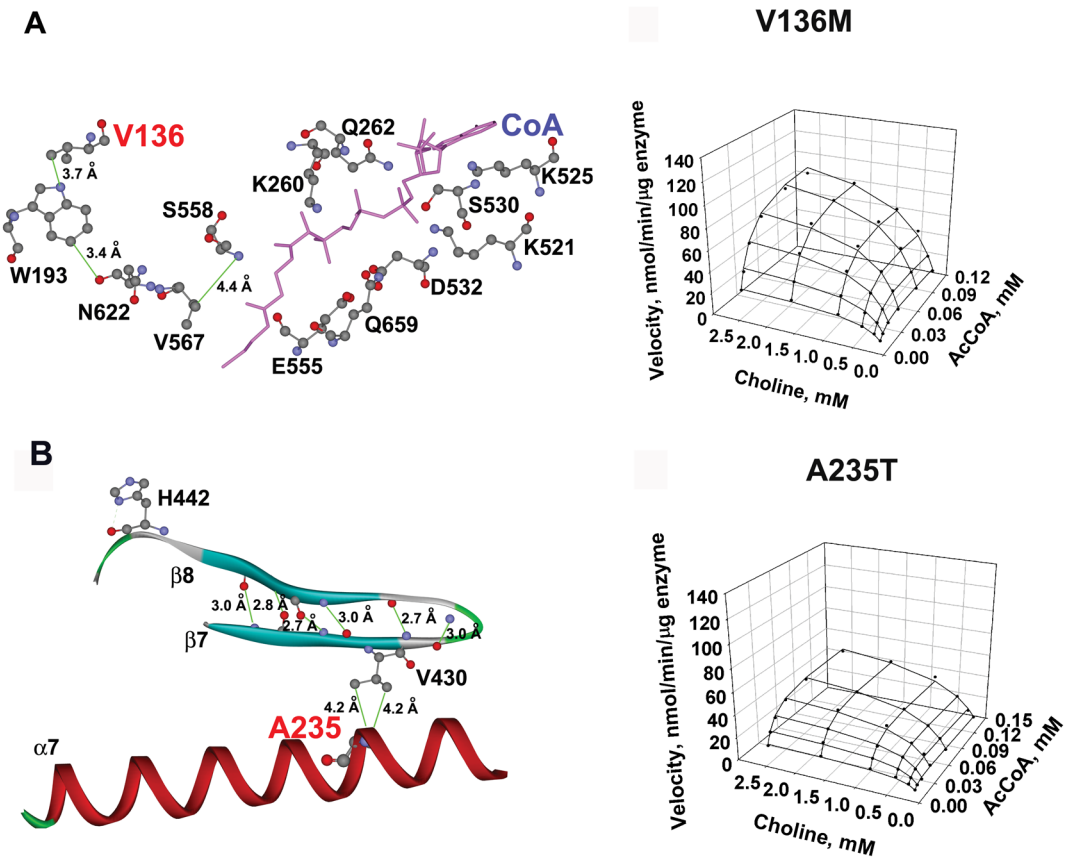

Fig. 5.

(A) Position of Val136 and kinetic landscape of p.Val136Met-ChAT. The main effect of the mutation is to enhance dissociation of AcCoA from the enzyme-substrate complex by 3-fold. (B) Position of Ala235 and the kinetic landscape of p.Ala235Thr-ChAT. The mutation decreases k_{cat} to 40% of wild-type. It is predicted to displace the antiparallel β strands 7 and 8, the latter connecting to His442.

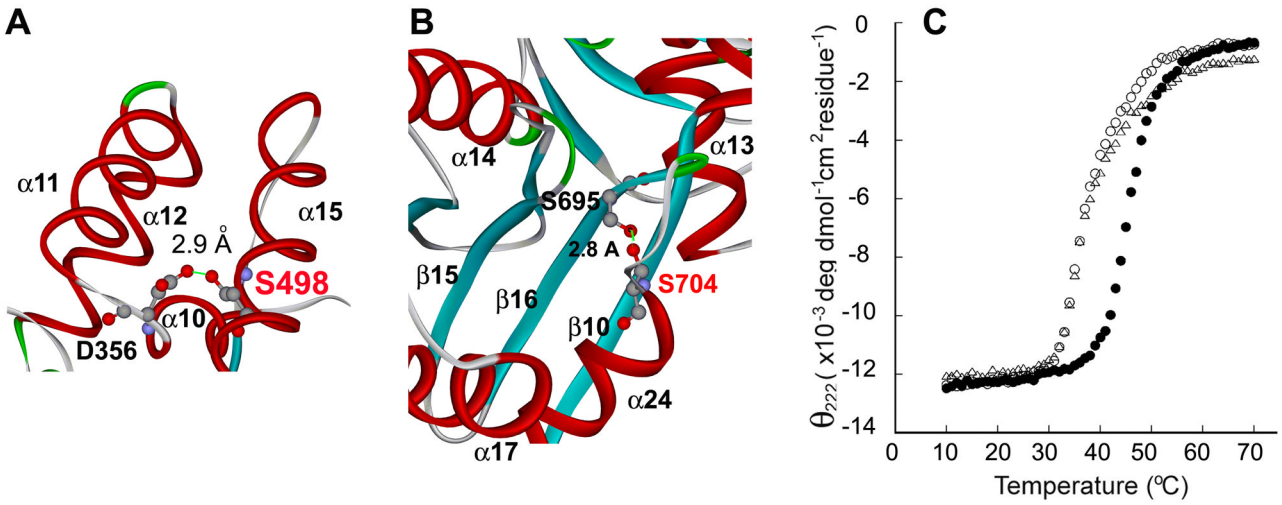

Fig. 6.

(A) Replacement of Ser498 by Pro on α-helix 15. (B) Replacement of Ser704 by Pro on α helix 24. (C) Thermal denaturation curves demonstrate altered conformational stability of the p.Ser498Pro (△) and p.Ser704Pro (○) mutants compared to wild-type ChAT (●). The circular dichroism of the different enzyme species is expressed as mean molar ellipticity per residue at a wavelength of 222 nm and is plotted as a function of temperature.

Table 1

Identified *CHAT* mutations

Patients	Nucleotide change[a]	Amino acid change	Major Effects
2, 6, 9	c.406G>A	p.Val136Met	Reduced expression, high K_{iA}
6	c.605T>G	p.Met202Arg	Very low k_{cat}, high K_{mA} and Ki_A
4	c.703G>A	p.Ala235Thr	Low k_{cat}
1	c.1262G>C	p.Trp421Ser	Very low expression, very low k_{cat}, high K_{iA}
3	c.1492T>C	p.Ser498Pro	Very low expression, high K_{iA}, large decrease in T_m
7	c.1658C>A	p.Thr553Asn	Low expression, low k_{cat}, very high K_{mA}, predicted very high K_{mB}, very high K_{iA}
10	c.1663G>T	p.Glu555X	Ablates large segment of binding and catalytic domains
3, 5, 8, 9, 10	c.1669G>A	p.Ala557Thr	Low expression, low k_{cat}, very high K_{mA} and K_{mB}
2	c.1715C>G	p.Ser572Trp	Very low expression, very low k_{cat}, very high K_{mA} and K_{mB}
4	c.1823C>A	p.Thr608Asn	Very high K_{ia}
1	c.1891G>A	p.Ala631Thr	Reduced expression, high K_{mA}
11	c.2066T>G	p.Ile689Ser	Reduced expression, low k_{cat}
7	c.2110T>C	p.Ser704Pro	Large decrease in T_m

[a]Nucleotide numbers start from the translational start site of the M type *CHAT* cDNA encoding 83 kDa ChAT, with +1 corresponding to the A of the ATG translation initiation codon according to reference sequence NM_ 020549.4; codon numbers start from the translation initiation codon according to the reference sequence NP_065574.

Abbreviations: k_{cat}, catalytic rate; K_{mA} and K_{mB}, Michaelis-Menten constants for AcCoA and choline; K_{iA}, dissociation constant for AcCoA from enzyme complex; T_m, thermal denaturation temperature.

Table 2

Kinetic parameters, thermal stabilities, and expression levels of wild-type and mutant ChAT enzymes

	k_{cat}, s^{-1}	K_{mA}, μM	K_{mB}, μM	K_{iA}, μM	k_{cat}/K_{mA} [a]	k_{cat}/K_{mB} [a]	$k_{cat}/K_{iA}K_{mB}$ [a]	T_m (°C)	Expression level
Wild-type	195 ± 5	11.9 ± 0.8	257 ± 32	3.7 ± 1.5	1.00	1.00	1.00	45.3 ± 0.08	1.00
p.Val136Met	167 ± 5[f]	14.4 ± 1.1	314 ± 49	11 ± 3.1[h]	0.71	0.70	0.24	43.9 ± 0.07	0.70 ± 0.06[h]
p.Met202Arg	5 ± 0.1[f]	32.0 ± 1.6[f]	223 ± 31	7.6 ± 2.8	0.009	0.03	0.01	ND	0.85 ± 0.09
p.Ala235Thr	84 ± 3 [f]	10.6 ± 0.9	315 ± 38	2.9 ± 1.4	0.48	0.35	0.45	43.9 ± 0.09	0.92 ± 0.07
p.Trp421Ser	0.12 ± 4E-3[f]	14.7 ± 1.0	220 ± 40	15 ± 4.5[h]	5E-4	7E-4	2E-4	ND	0.19 ± 0.02[f]
p.Ser498Pro	141 ± 3 [f]	9.3 ± 0.6[h]	203 ± 28	7.3 ± 2.1	0.93	0.92	0.47	37.8 ± 0.22	0.31 ± 0.04 [f]
p.Thr553Asn	127 ± 3[b,f]	98.8[b]	ND[c]	29 ± 6.0[f]	0.08	0.09	ND[c]	ND	0.41 ± 0.02 [f]
p.Ala557Thr	130 ± 2[b,f]	98.8[b]	ND[c]	33 ± 6.0[f]	0.08	0.09	ND[c]	ND	0.42 ± 0.04 [f]
p.Ser572Trp	29 ± 2[d,f]	ND[e]	2,500[d]	ND[e]	0.04	0.02	ND[e]	ND	0.26 ± 0.03 [f]
p.Thr608Asn	162 ± 5[f]	17.2 ± 1.2[f]	163 ± 16[g]	13 ± 2.9[g]	0.58	1.31	0.39	46.2 ± 0.07	1.23 ± 0.15
p.Ala631Thr	179 ± 11	16.6 ± 2.0[h]	438 ± 93	2.8 ± 2.1	0.66	0.54	0.71	44.6 ± 0.08	0.70 ± 0.02 [f]
p.Ile689Ser	53 ± 2[f]	9.0 ± 0.7[g]	275 ± 42	3.7 ± 1.9	0.36	0.25	0.25	43.9 ± 0.14	0.52 ± 0.01[f]
p.Ser704Pro	184 ± 5	11.4 ± 0.9	283 ± 38	3.6 ± 1.6	0.98	0.86	0.88	37.5 ± 0.22	0.83 ± 0.05

Codon numbers start from the ATG translation initiation codon according to reference sequence NP_065574. Values indicate mean ± SE. Standard errors in kinetic parameters of ChAT were obtained through weighted nonlinear regression analysis of 12 curves derived from a 36-point assay by estimating the covariance matrix as implemented in Sigmaplot 10. The SE of the melting point, T_m, for each mutant is that of the sigmoidal function estimated from nonlinear regression analysis preformed by KaleidaGraph (Synergy Software). The standard error for expression levels indicate results of 3 to 4 transfections.

Abbreviations: k_{cat}, turnover number; K_{mA}, Michaelis-Menten constants for AcCoA; K_{mB}, Michaelis-Menten constants for choline; K_{iA}, dissociation constant for enzyme-AcCoA complex; T_m, thermal denaturation temperature.

[a] Catalytic efficiency for AcCoA (k_{cat}/K_{mA}) and for choline (k_{cat}/K_{mB}), and the overall catalytic efficiency $k_{cat}/(K_{iA}K_{mB})$ are normalized with respect to wild-type. In wild-type, k_{cat}/K_{mA} = 16.41×10^{6} $s^{-1}M^{-1}$, k_{cat}/K_{mB} = 7.6×10^{5} $s^{-1}M^{-1}$, $k_{cat}/(K_{iA}K_{mB})$ = 2.05×10^{11} $s^{-1}\cdot M^{-2}$, and $k_{cat}/(K_{mA}K_{mB})$ = 6.38×10^{10} $s^{-1}M^{-2}$.

[b] Apparent values calculated at 2.5 mM choline.

[c] Not determined because K_{mB} exceeds practical concentration range of choline. Catalytic efficiency was calculated from Eq. 3 in Methods.

[d] Apparent values calculated at 116 μM AcCoA.

[e] Not determined because K_{mA} exceeds practical concentration range of AcCoA. Catalytic efficiency was calculated from Eq. 4 in Methods.

[f,g,h] $P < 0.001$, 0.01, 0.05, respectively.